DNA Nanotechnology

International Edition: DOI: 10.1002/anie.201604621
German Edition: DOI: 10.1002/ange.201604621

DNA Origami Rotaxanes: Tailored Synthesis and Controlled Structure Switching

*John T. Powell, Benjamin O. Akhuetie-Oni, Zhao Zhang, and Chenxiang Lin**

Abstract: *Mechanically interlocked supramolecular assemblies are appealing building blocks for creating functional nanodevices. Herein, we describe the multistep assembly of large DNA origami rotaxanes that are capable of programmable structural switching. We validated the topology and structural integrity of these rotaxanes by analyzing the intermediate and final products of various assembly routes by electrophoresis and electron microscopy. We further analyzed two structure-switching behaviors of our rotaxanes, which are both mediated by DNA hybridization. In the first mechanism, the translational motion of the macrocycle can be triggered or halted at either terminus. In the second mechanism, the macrocycle can be elongated after completion of the rotaxane assembly, giving rise to a unique structure that is otherwise difficult to access.*

Supramolecular assemblies with mechanically interlocked components are of considerable interest to nanorobotics and nanomechanics.[1] One such mechanically bonded assembly is the rotaxane, a dumbbell-shaped molecule whose central axle is threaded through a ring- or tube-shaped macrocyclic molecule.[2] Owing to the translational and rotational freedom of the macrocycle, rotaxanes harbor potential as molecular switches and/or molecular cargo shuttles; their movement can be dictated by various chemical stimuli, including addition of DNA strands, pH changes, and light signals.[3] Intrigued by the potential applications of rotaxanes as stimulus-responsive switches and the diverse conjugation chemistry compatible with DNA nanodevices,[4] several recent investigations have focused on the assembly of rotaxanes from DNA.[3b,5]

Inspired by these antecedent DNA rotaxanes, the rapidly expanding catalogue of dynamic DNA origami devices,[6] and demonstrations of multimeric DNA origami assembly through shape-complementary topologies,[7] we herein present a strategy for assembling a rotaxane from three DNA origami structures. The large size, thermal stability, and DNA-induced macrocycle switching and reconfiguration are the most distinguishable features of this nanodevice compared to previous DNA rotaxanes.

Our rotaxane (R) is composed of three scaffolded DNA origami[8] monomers, namely a macrocycle (M) and two half-dumbbells (dL and dS), which were all designed using caDNAno software (see the Supporting Information, Figure S1).[9] The square-shaped macrocycle (35 nm × 35 nm × 27.5 nm, length × width × height) displays four 16-nm, four-helix bundle rods radiating outwards from the four sides of the square (Figure 1 and Figure S2-1). The dL and dS monomers (Figure 1 and Figure S2-2) are structurally identical, each consisting of a square-shaped stopper (35 nm × 35 nm × 17.5 nm) suspended on an eight-helix bundle axle (7.5 nm × 7.5 nm × 96 nm) by four pairs of single-stranded DNA tendons (35 nt stretched over 9.8 nm), each exerting a tension force of about 6 pN as predicted by a modified freely jointed chain model.[10] The unsymmetric half-dumbbells each feature a short axle end and a long axle end. The macrocycle M and each of the half-dumbbell stoppers possess a pair of notched surfaces (highlighted in yellow and red, respectively, in Figure 1 and Figure S2) that allow for stacking in the presence of sequence-specific linking DNA strands. In this work, we designed two sets of linking strands X and Y, which dock M to the short- or long-axle facing side of the stopper, respectively. All linking strands carry a 6-nt extension, or DNA toehold, to facilitate the release of M at a later stage. For example, M can be docked to the short-axle-facing side of the stopper on dL by linking strand set X, giving rise to

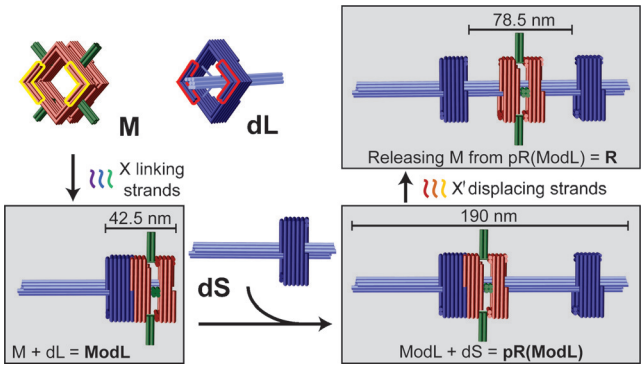

Figure 1. DNA origami rotaxane components and a viable three-step assembly route. Each cylinder represents a DNA double helix. DNA origami monomers (macrocycle M and half-dumbbell dL) are shown in the top left corner. Notches on the top faces of M and dL are highlighted in yellow and red, respectively; their bottom faces have notches of complementary shape. Intermediate and final products are shown in gray boxes.

[*] J. T. Powell, Dr. Z. Zhang, Prof. C. Lin
Department of Cell Biology & Nanobiology Institute
Yale University
850 West Campus Drive, West Haven, CT 06516 (USA)
E-mail: chenxiang.lin@yale.edu
B. O. Akhuetie-Oni
Department of Molecular, Cellular, and Developmental Biology & Nanobiology Institute, Yale University
850 West Campus Drive, West Haven, CT 06516 (USA)

Supporting information for this article can be found under: http://dx.doi.org/10.1002/anie.201604621.

a dimeric assembly intermediate ModL (M on dL) as shown in the bottom left box of Figure 1. Furthermore, one end of each half-dumbbell axle (the long end of dL and the short end of dS) was rendered inert (i.e., incapable of dimerization) while the other end was functionalized with DNA extensions to facilitate end-to-end binding between the two half-dumbbells. Therefore, reacting dS with ModL can in principle produce a second assembly intermediate pR(ModL), which is a pseudo-rotaxane (Figure 1, bottom right). This intermediate can subsequently be converted into a genuine rotaxane (R) by releasing M through toehold-mediated strand displacement[11] upon addition of a displacing strand set X′ that binds the linking strand set X (Figure 1, top right).

We utilized agarose gel electrophoresis, gel extraction, and negative-stain transmission electron microscopy (TEM) to identify components of the three assembly steps (Figure 2a; see also Figures S3 and S4). The first assembly reaction (rA) consisted of M and dL in equimolar amounts and a 60-fold excess of the linking strand set X, and it was incubated at 40 °C for 16 h. The gel lane containing the rA mixture showed only one major band aside from those of the reactants; gel extraction and TEM revealed that this band contained the correctly formed dimer ModL and misassembled dimers that we termed ModL*. The second reaction (rB) mixture consisted of the unpurified rA mixture with dS added in equimolar amount to dL; the reaction was incubated at 40 °C for 16 h. Gel electrophoresis of the rB mixture showed a new band in addition to the monomer and dimer bands. Analyzing the extract of this slower band by TEM revealed the pseudo-rotaxane pR(ModL) and its misassembled counterparts pR(ModL)*. The final assembly step (rC) was to incubate the rB mixture with a 5-fold excess (relative to the linking strand set X) of displacing strand set X′ at 44 °C for 12 h. Electrophoresis yielded a similar band pattern as for rB but with reduced intensity of the trimer band, suggesting that only some trimers formed in rB retained the same molecular weight after releasing M. Despite minor structural damage during gel extraction (giving rise to small amounts of the monomers and dimers), TEM analysis confirmed that all trimeric structures containing M within this band were genuine rotaxane R, in which the macrocycle sat between the stoppers with the axle threading through all three squares. Note that the rods and the thickness of M distinguish it from the stoppers of dL or dS in TEM images.

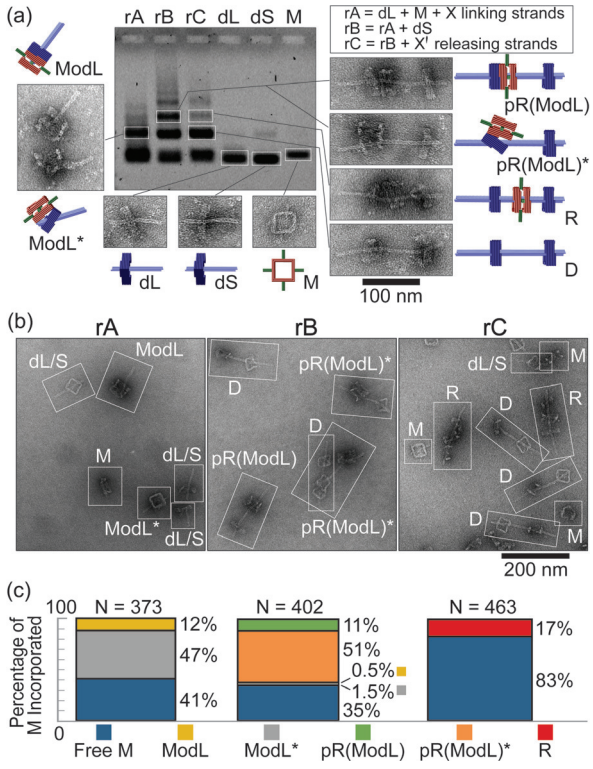

Figure 2. DNA origami rotaxane assembly products. a) Agarose gel electrophoresis showing individual assembly components and reaction mixtures after each assembly step. The reactants of each assembly step (rA, rB, and rC) are listed in the box in the top right corner. Representative close-up TEM images of the extracted bands of interest are shown along with schematic representations. b) Representative zoom-out TEM images of the unpurified reaction mixtures. Each distinguishable nanostructure was identified and labeled with an abbreviation. c) The macrocycle incorporation efficiency after each reaction step. The stacked bars from left to right correspond to rA, rB, and rC, respectively.

To quantify the efficiency of each assembly step, we analyzed TEM images of the unpurified assembly products of rA, rB, and rC (Figure 2b). After categorizing and counting all resolvable nanostructures, we determined the assembly efficiency as a measure of the assembly state of M at the end of each step (Figure 2c). Statistics ($N = 463$) indicated that approximately 17 % of M were incorporated into the intended product R after the three-step assembly. We considered two possible reasons for this low yield. One possibility is that the macrocycles of many pseudo-rotaxanes dethreaded from their axles following strand displacement because of thermal instability (e.g., two dumbbell halves temporarily detached). However, properly assembled rotaxanes stayed intact when incubated at room temperature for over a month or at 44 °C for 20 h (Figure S5), which spoke against this hypothesis. An alternative and more likely explanation is that the yield of R was limited by the macrocycle threading efficiency during rA. Hence, the intermediates ModL* and pR(ModL)* were considered to be malformed assemblies in which M did not fully thread over the axle of dL; the release of M from pR(ModL)* necessarily yielded empty dumbbells (D) and monomeric macrocycles. Indeed, the assembly efficiency of the two properly formed intermediates (12 % for ModL and 11 % for pR(ModL)) roughly equaled that of the rotaxane (17 %); the chances of M being incorporated in misassembled intermediates in the first two assembly steps also matched well (47 % ModL* and 51 % for pR(ModL)*). The discrepancies in the percentages were likely due to structural distortion on the TEM grid, mainly the flattening of the M-docked stopper in 24–29 % of the nanostructures containing M (Figure S6), which we interpreted as misfolded intermediates, leading to an underestimation of correctly formed ModL and pR(ModL).

As our TEM images only resolve the two-dimensional projections of the three-dimensional DNA nanostructures, we designed two more experiments to probe the topology of the

rotaxanes. In the first experiment, we added M and linking strands (set X) to the preassembled dumbbells. Although we found DNA origami trimers akin to pR(ModL)*, releasing M did not result in any rotaxane detectable by TEM (Figure S7). This confirmed that full threading of the macrocycle over the axle cannot occur after dumbbell formation. In other words, the dumbbell stoppers present insurmountable barriers to any macrocycle. In the second experiment, our attempts to assemble rotaxanes by first docking M to the long-axle-facing side of the dS stopper (i.e., M + dS + linking strand set Y) eventually produced negligible amounts of R (Figure S8). Notably, all intermediate products appeared to be improperly formed such that the axle did not penetrate through M. This result suggested that proper threading is critical for the formation of R and further supported that the initial docking of M on dS or dL is the yield-limiting step. We speculated that the difference between threading M over the long versus the short axle can be attributed to a hinging–clamping process. According to this speculation, part of the docking interface of the macrocycle can first bind with a stopper (hinging step), which does not entail threading over the axle; the rest of the interface can then engage in a clamping motion, latching M onto the half-dumbbell. The latter requires an axle that is shorter than the macrocycle width (Figure S9). The hypothetical partial docking state can in principle lower the entropic barrier ordinarily present when randomly threading a ring over a rod (Figure S10),[12] which could explain the dismal yield of R when the assembly cannot benefit from this stepping stone (e.g., when threading M through the long axle end or adding M to a half-dumbbell without linking strands). Combining the findings described above, we have established the mechanically locked state of the macrocycle within a structurally stable DNA origami rotaxane.

The free movement of macrocycles between stoppers is the hallmark of rotaxanes. We examined the macrocycle's translational motion by recording the position of M in relation to either dumbbell stopper for each rotaxane identified by TEM. We measured the center-to-center distances of i) M to the dL stopper, ii) M to the dS stopper, and iii) stopper to stopper. We then defined the relative position of M as (i)/(iii) or (ii)/(iii). By plotting the relative macrocycle positions of 252 rotaxanes as histograms (Figure 3a), we found that nearly all ($\geq$246 out of 252) normalized values fell between 0.21 and 0.79 with a mean close to 0.5, as dictated by the designed dimensions of the rotaxane (Figure S11). The data further suggested that the macrocycles were equally likely to sit at any given position in the middle third of the axle (between 0.34 and 0.66); however, the frequency of M residing beyond these points tapered off rapidly towards the stoppers. In light of the tilting flexibility of the dumbbell stoppers as seen in the TEM images, we reasoned that the loss of probability density in these regions (clash zones) is due to steric hindrance posed to the macrocycle by the wobbly stoppers (Figure S12). Stopper wobbling may also explain why slightly more M stayed close to the dL stopper since the dS stopper is expected to be more flexible due to its proximity to the axle end.

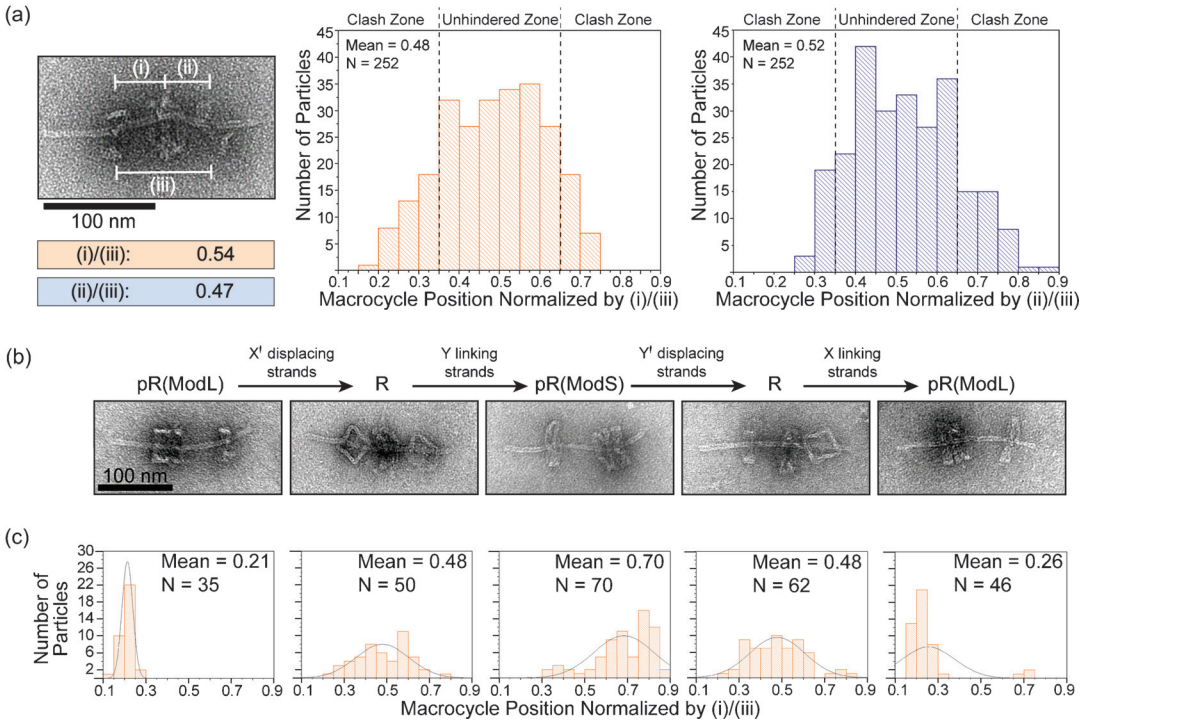

Figure 3. The movement and switching of macrocycles in DNA origami rotaxanes. a) Distribution of the macrocycle positions with respect to the stoppers. Left: Close-up TEM image and normalized macrocycle position of an exemplary rotaxane. Center and right: Normalized macrocycle positions plotted as histograms; note that although the two histograms are based on the same TEM images, they are not perfect mirror images owing to slight bending of the rotaxane axles. b) Top: Scheme of rotaxane structural switching induced by displacing or linking strands. Bottom: Close-up TEM images of the desired products. c) Distributions of the macrocycle positions resulting from the switching operations. The histograms correspond to the switching states in (b). The superimposed curves are included only as a guide to the eye.

After validating that the macrocycle translates freely, we examined the potential of our rotaxane as a molecular switching device. As shown in Figure 3b and c, the rotaxane responded correctly to the appropriate displacing and linking strands and switched reversibly between its free state R and two stopper-docked states, pR(ModL) and pR(ModS). A caveat of the device was the incomplete switching to the pR(ModS) state (i.e., a pseudo-rotaxane with M on dS, see Figure 3c, middle). The reason for this inefficiency may be the orientation variability of the stopper, meaning that some of the half-dumbbells bear a stopper facing the wrong direction. In fact, we noticed that dS sometimes docked with M on the side opposite to our design during our attempts to form pR(ModS) both through switching and through direct assembly (Figure S13); the latter case lowered the yield of R. Thus we suspected that the portion of R incapable of assuming the pR(ModS) state likely contained such misfolded dS. Nevertheless, the abilities of the macrocycle to slide freely and change docking position in response to chemical cues are promising features for the future development of molecular switches and shuttles.

Finally, we demonstrated that we can obtain rotaxanes of different macrocycle-threading topologies through varied assembly pathways. To show this, we utilized a macrocycle with single-stranded scaffold DNA loops connecting two squares. This macrocycle, M_{Short} (thickness: 30.9 ± 11.5 nm), can be converted into a 62.5 nm long macrocycle (M_{Long}) with the addition of an auxiliary set of 60 staple strands (Figure 4a). Rotaxanes containing the short macrocycle (termed $R(M_{Short})$) were formed with similar efficiency to the original rotaxane R as assessed by negative-stain TEM (Figure 4b and Figure S14). Following this assembly, we added the auxiliary staple set to the reaction mixture and annealed the entire reaction from 40 to 20 °C over 18 h. Rotaxanes generated this way contained tubular macrocycles (M_{Long}) with both squares threaded over the axle ($R(M_{Long}2)$, see Figure 4b); $R(M_{Long}2)$ was the major rotaxane product (88%) of such an on-axle structural switching procedure. When we assembled rotaxanes with premade M_{Long}, another unique rotaxane, $R(M_{Long}1)$, consistently emerged (96% of all rotaxanes), with only one square of the macrocycle threaded and the other one left unthreaded (Figure 4c).

In conclusion, we have constructed a class of DNA origami rotaxanes. The yield and quality of these rotaxanes have much room for improvement (e.g., by rigidifying the connections between stopper and axle to limit the tilting flexibility of the stopper or by purifying the desired product after each assembly step). However, the rotaxanes presented here are larger and more rigid than antecedent interlocked DNA nanodevices and harbor great potential for functionalization with a myriad of biomolecule cargos (e.g., proteins) and stimulus-responsive components. Moreover, the modular design and structure-switching properties of the rotaxanes open up new possibilities for producing otherwise entropically unfavorable DNA structures and for programmably altering rotaxane geometry and dynamics. Simmel and coworkers recently made several multicomponent rotaxanes using a different assembly scheme.[13]

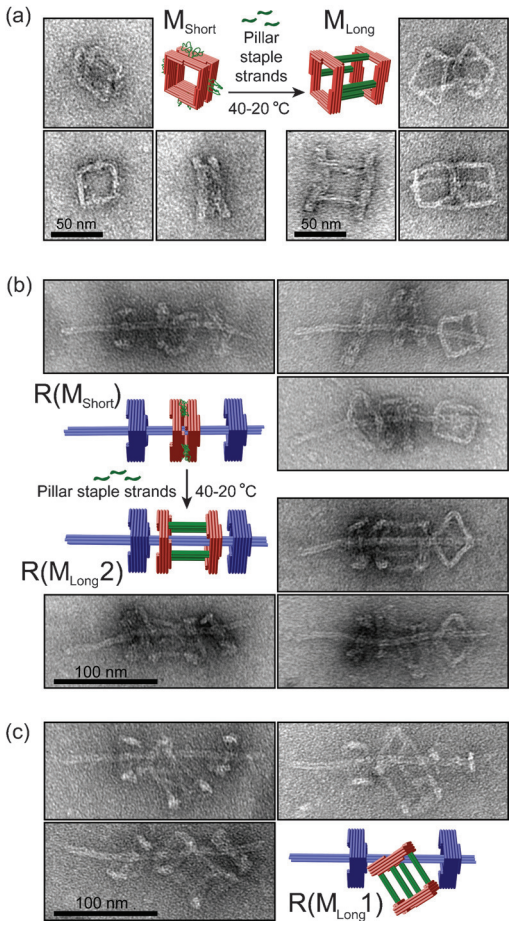

Figure 4. Assembling DNA origami rotaxanes with a tubular macrocycle. a) Structural reconfiguration of a macrocycle by folding its unpaired scaffold loops into rigid four-helix bundle pillars. Close-up TEM images show the typical appearances of monomeric macrocycles before and after reconfiguration. b) Elongating a macrocycle of a complete DNA rotaxane. Close-up TEM images show the typical appearances of rotaxanes before and after reconfiguration. c) Rotaxanes assembled using an elongated tubular macrocycle as a starting component. Note the different topologies of the rotaxanes shown in (b) and (c).

Acknowledgements

This work was supported by a National Institutes of Health (NIH) Director's New Innovator Award (DP2-GM114830), an NIH grant (R21-GM109466), and a Yale University faculty startup fund to C.L. Additionally, J.T.P. and B.O.A.-O. are supported by NIH training grants (T32-GM067543 and T32-GM007223, respectively).

Keywords: DNA nanotechnology · DNA origami · macrocycles · molecular devices · rotaxanes

How to cite: *Angew. Chem. Int. Ed.* **2016**, *55*, 11412–11416
Angew. Chem. **2016**, *128*, 11584–11588

[1] a) C. Cheng, J. F. Stoddart, *ChemPhysChem* **2016**, *17*, 1780–1793; b) X. Liu, C. H. Lu, I. Willner, *Acc. Chem. Res.* **2014**, *47*, 1673–1680; c) C. H. Lu, A. Cecconello, I. Willner, *J. Am. Chem.*

Soc. **2016**, *138*, 5172 – 5185; d) C. A. Schalley, K. Beizai, F. Vogtle, *Acc. Chem. Res.* **2001**, *34*, 465 – 476.
[2] I. T. Harrison, S. Harrison, *J. Am. Chem. Soc.* **1967**, *89*, 5723 – 5724.
[3] a) F. Lohmann, D. Ackermann, M. Famulok, *J. Am. Chem. Soc.* **2012**, *134*, 11884 – 11887; b) F. Lohmann, J. Weigandt, J. Valero, M. Famulok, *Angew. Chem. Int. Ed.* **2014**, *53*, 10372 – 10376; *Angew. Chem.* **2014**, *126*, 10540 – 10544; c) P. Waeles, B. Riss-Yaw, F. Coutrot, *Chem. Eur. J.* **2016**, *22*, 6837 – 6845.
[4] a) M. R. Jones, N. C. Seeman, C. A. Mirkin, *Science* **2015**, *347*, 1260901; b) B. Saccà, C. M. Niemeyer, *Chem. Soc. Rev.* **2011**, *40*, 5910 – 5921; c) Y. R. Yang, Y. Liu, H. Yan, *Bioconjugate Chem.* **2015**, *26*, 1381 – 1395.
[5] a) D. Ackermann, S. S. Jester, M. Famulok, *Angew. Chem. Int. Ed.* **2012**, *51*, 6771 – 6775; *Angew. Chem.* **2012**, *124*, 6875 – 6879; b) D. Ackermann, T. L. Schmidt, J. S. Hannam, C. S. Purohit, A. Heckel, M. Famulok, *Nat. Nanotechnol.* **2010**, *5*, 436 – 442; c) J. Valero, F. Lohmann, D. Keppner, M. Famulok, *ChemBioChem* **2016**, *17*, 1146; d) J. Weigandt, C. L. Chung, S. S. Jester, M. Famulok, *Angew. Chem. Int. Ed.* **2016**, *55*, 5512 – 5516; *Angew. Chem.* **2016**, *128*, 5602 – 5606.
[6] a) E. S. Andersen et al., *Nature* **2009**, *459*, 73 – 76; b) S. M. Douglas, I. Bachelet, G. M. Church, *Science* **2012**, *335*, 831 – 834; c) Y. Ke, T. Meyer, W. M. Shih, G. Bellot, *Nat. Commun.* **2016**, *7*, 10935; d) P. Ketterer, E. M. Willner, H. Dietz, *Sci. Adv.* **2016**, *2*, e1501209; e) A. E. Marras, L. Zhou, H. J. Su, C. E. Castro, *Proc. Natl. Acad. Sci. USA* **2015**, *112*, 713 – 718.
[7] a) T. Gerling, K. F. Wagenbauer, A. M. Neuner, H. Dietz, *Science* **2015**, *347*, 1446 – 1452; b) S. Woo, P. W. Rothemund, *Nat. Chem.* **2011**, *3*, 620 – 627.
[8] a) S. M. Douglas, H. Dietz, T. Liedl, B. Hogberg, F. Graf, W. M. Shih, *Nature* **2009**, *459*, 414 – 418; b) P. W. Rothemund, *Nature* **2006**, *440*, 297 – 302.
[9] S. M. Douglas, A. H. Marblestone, S. Teerapittayanon, A. Vazquez, G. M. Church, W. M. Shih, *Nucleic Acids Res.* **2009**, *37*, 5001 – 5006.
[10] T. Liedl, B. Hogberg, J. Tytell, D. E. Ingber, W. M. Shih, *Nat. Nanotechnol.* **2010**, *5*, 520 – 524.
[11] D. Y. Zhang, G. Seelig, *Nat. Chem.* **2011**, *3*, 103 – 113.
[12] E. M. Sevick, D. R. Williams, *Nano. Lett.* **2016**, *16*, 671 – 674.
[13] J. List, E. Falgenhauer, E. Kopperger, G. Pardatscher, F. C. Simmel, *Nat. Commun.* **2016**, *7*, 12414.

Received: May 18, 2016
Revised: July 8, 2016
Published online: August 16, 2016

